J|A|C|S
ARTICLES
Published on Web 04/03/2002

The $[Sn_9Pt_2(PPh_3)]^{2-}$ and $[Sn_9Ni_2(CO)]^{3-}$ Complexes: Two Markedly Different Sn_9M_2L Transition Metal Zintl Ion Clusters and Their Dynamic Behavior

Banu Kesanli, James Fettinger, Donna R. Gardner, and Bryan Eichhorn*

Contribution from the Department of Chemistry and Biochemistry, University of Maryland, College Park, Maryland 20742

Received November 13, 2001

Abstract: $[Sn_9Pt_2(PPh_3)]^{2-}$ (**2**) was prepared from $Pt(PPh_3)_4$, K_4Sn_9, and 2,2,2-cryptand in en/toluene solvent mixtures. The $[K(2,2,2\text{-cryptand})]^+$ salt is very air and moisture sensitive and has been characterized by ESI-MS, variable-temperature ^{119}Sn, ^{31}P, and ^{195}Pt NMR and single-crystal X-ray diffraction studies. The structure of **2** comprises an elongated tricapped Sn_9 trigonal prism with a capping $PtPPh_3$, an interstitial Pt atom, a *hypercloso* electron count (10 vertex, 20 electron) and C_{3v} point symmetry. Hydrogenation trapping experiments and deuterium labeling studies showed that the formation of **2** involves a double C−H activation of solvent molecules (en or DMSO) with the elimination of H_2 gas. The ESI-MS analysis of **2** showed the $K[Sn_9Pt_2(PPh_3)]^{1-}$ parent ion, an oxidized $[Sn_9Pt_2(PPh_3)]^{1-}$ ion, and the protonated binary cluster anion $[HSn_9Pt_2]^{1-}$. **2** is highly fluxional in solution giving rise to a single time-averaged ^{119}Sn NMR signal for all nine Sn atoms but the Pt atoms remain distinct. The exchange is intramolecular and is consistent with a rigid, linear Pt−Pt−PPh_3 rod embedded in a liquidlike Sn_9 matrix. $[Sn_9Ni_2(CO)]^{3-}$ (**3**) was prepared from $Ni(CO)_2(PPh_3)_2$, K_4Sn_9, and 2,2,2-cryptand in en/toluene solvent mixtures. The $[K(2,2,2\text{-cryptand})]^+$ salt is very air and moisture sensitive, is paramagnetic, and has been characterized by ESI-MS, EPR, and single-crystal X-ray diffraction. Complex **3** is a 10-vertex 21-electron polyhedron, a slightly distorted *closo*-Sn_9Ni cluster with an additional interstitial Ni atom and overall C_{4v} point symmetry. The EPR spectrum showed a five-line pattern due to 4.8-G hyperfine interactions involving all nine tin atoms. The ESI-MS analysis showed weak signals for the potassium complex $[K_2Sn_9Ni_2(CO)]^{1-}$ and the ligand-free binary ions $[K_2Sn_9Ni_2]^{1-}$, $[KSn_9Ni_2]^{1-}$, and $[HSn_9Ni_2]^{1-}$.

Introduction

The chemistry of the group 14 $E_9^{3-/4-}$ Zintl ions (E = Ge, Sn, Pb) is of growing interest due to the remarkable basic chemistry associated with these clusters[1−9] and their potential utility in preparing ligand-free nanomaterials.[2] Sn_9^{4-} adopts a discrete 9-vertex, 22-electron structure[10−12] with C_{4v} point symmetry (see **I**) and is classified as a *nido*-cluster type

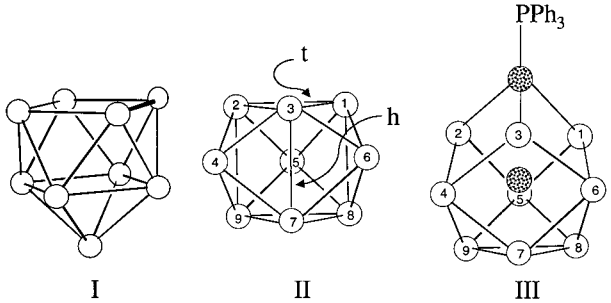

I II III

according to Wade's rules.[13] Rudolph and co-workers studied the solution dynamics of *nido*-Sn_9^{4-} by way of ^{119}Sn NMR spectroscopy.[14] Their studies showed that, unlike the isoelectronic boranes, *nido*-Sn_9^{4-} is highly fluxional in solution such that all nine Sn atoms are in rapid exchange on the NMR time scale at −74 °C. The presence and intensity of ^{117}Sn satellites on the lone resonance indicates that the exchange is intramolecular[12,15] and involves a bond-making step across the open face of the cluster along with a bond-breaking process.[11,12]

Structurally characterized metalated polystannides have been prepared by various means and include the complexes *closo*-$[Sn_9M(CO)_3]^{4-}$, where M = Cr, Mo, W,[16−18] *closo*-{$[Sn_6[Cr$-

(1) Fassler, T. F. *Angew. Chem., Int. Ed.* **2001**, *40*, 4161.
(2) Fassler, T. F. *Coord. Chem. Rev.* **2001**, *215*, 347.
(3) Fassler, T. F.; Hunziker, M.; Spahr, M. E.; Lueken, H.; Schilder, H. *Z. Anorg. Allg. Chem.* **2000**, *626*, 692.
(4) Fassler, T. F.; Hoffmann, R. *Z. Kristallogr. New Cryst. Struct.* **2000**, *215*, 139.
(5) Fassler, T. F.; Hoffmann, R. *J. Chem. Soc., Dalton Trans.* **1999**, 3339.
(6) Fassler, T. F.; Hunziker, M. *Inorg. Chem.* **1994**, *33*, 5380.
(7) Fassler, T. F.; Muhr, H. J.; Hunziker, M. *Eur. J. Inorg. Chem.* **1998**, 1433.
(8) Critchlow, S. C.; Corbett, J. D. *J. Am. Chem. Soc.* **1983**, *105*, 5715.
(9) Campbell, J.; Dixon, D. A.; Mercier, H. P. A.; Schrobilgen, G. J. *Inorg. Chem.* **1995**, *34*, 5798.
(10) Diehl, L.; Khodadedeh, K.; Kummer, D.; Strähle, J. *Chem. Ber.* **1976**, *109*, 3404.
(11) Corbett, J. D.; Edwards, P. A. *J. Am. Chem. Soc.* **1977**, *99*, 3313.
(12) Corbett, J. D. *Chem. Rev.* **1985**, *85*, 383.
(13) Wade, K. J. *Adv. Inorg. Chem. Radiochem.* **1976**, *18*, 1.
(14) Rudolph, R. W.; Wilson, W. L.; Parker, F.; Taylor, R. C.; Young, D. C. *J. Am. Chem. Soc.* **1978**, *100*, 4629.
(15) Wilson, W. L.; Rudolph, R. W.; Lohr, L. L.; Taylor, R. C.; Pyykko, P. *Inorg. Chem.* **1986**, *25*, 1535.
(16) Kesanli, B.; Fettinger, J. C.; Gardner, D. R.; Eichhorn, B. W. *Chem.−Eur. J.* **2001**, 5277.

$(CO)_5]_6\}^{2-}$,[19,20] and $[(\eta\text{-}C_7H_8)Nb(cyclo\text{-}Sn_6)Nb(\eta\text{-}C_7H_8)]^{2-}$.[21] The latter two complexes are static on the NMR time scale,[20] as expected, and show one-bond Sn−Sn coupling constants significantly larger that those of *nido*-Sn_9^{4-}.[12,15] Surprisingly, the *closo*-$[Sn_9M(CO)_3]^{4-}$ complexes show local fluxionality that remains rapid on the NMR time scale at −50 °C.[16]

Rudolph and co-workers[22] prepared the first metalated Zintl ion, a Sn_9^{4-} - - $Pt(PPh_3)_x$ complex, which was characterized by ^{119}Sn NMR spectroscopy. The presence of ^{195}Pt−^{119}Sn coupling observed in the room-temperature ^{119}Sn NMR spectrum indicates that the $Pt(PPh_3)_x$ fragment is not dissociating from the Sn_9 cluster on the NMR time scale. However, the complex is highly fluxional and shows a single time-averaged chemical shift for the nine tin atoms.[22] Because the composition and structure of the complex remain unknown, one cannot speculate about the mechanism of the dynamic behavior. It was surprising to us that the proposed[22] *nido*-10-atom 24-electron cluster would retain dynamic behavior similar to *nido*-Sn_9^{4-} with global exchange of all nine Sn atoms. This observation prompted us to study the relationships between the structures of the metalated Sn_9 complexes and their dynamic behavior. Herein we describe the synthesis, structures, properties, and remarkable solution dynamics of two related metalated polystannides: $[Sn_9Pt_2(PPh_3)]^{2-}$ and $[Sn_9Ni_2(CO)]^{3-}$. The former possesses a highly distorted Sn_9 cluster and shows liquidlike behavior in solution whereas the latter possesses a C_{4v} *closo* structure and is a rare example of a paramagnetic Zintl complex.

Results

Synthesis. Ethylenediamine (en) or DMSO solutions of K_4Sn_9 react with toluene solutions of $Pt(PPh_3)_4$ in the presence of 2,2,2-cryptand to give moderate yields of the $[Sn_9Pt_2(PPh_3)]^{2-}$ ion (**2**) as the $[K(2,2,2\text{-crypt})]^+$ salt (eq 1). The formation of **2**

$$\underset{(\mathbf{1})}{Sn_9^{4-}} + 2Pt(PPh_3)_4 + 2en \xrightarrow{(2,2,2-crypt)} \underset{(\mathbf{2})}{[Sn_9Pt_2(PPh_3)]^{2-}} + 7PPh_3 + 2[H_2N(CH_2)_2NH]^{1-} + H_2 \quad (1)$$

requires a net two-electron oxidation of the starting materials that is accompanied by a two-electron reduction of solvent molecules. The formation of hydrogen gas in eq 1 was verified by a hydrogenation trapping experiment. A solution of *trans*-stilbene was hydrogenated to bibenzyl (eq 2) where the head

$$PhCH{=}CHPh + H_2 \xrightarrow{[Pd]/C} PhCH_2CH_2Ph \quad (2)$$

gases from eq 1 were used as the hydrogen source. The use of DMSO-d_6/tol solvent mixtures in eq 1 chemistry results in the formation of bibenzyl-d_2 as the only hydrogenation product. The use of tol-d_8 does not result in deuterium incorporation in the bibenzyl. The reduction of solvent molecules has been documented in the formation of the closely related $[E_7PtH(PPh_3)]^{2-}$ Zintl ions (E = P, As).[23] In the present reaction, a second molecule is reduced to give 1 equiv of H_2 according to eq 1.

The $[K(2,2,2\text{-crypt})]^+$ salt of **2** is very air and moisture sensitive in solution and the solid state. The salt is sparingly soluble in en and moderately soluble in DMF and CH_3CN and forms dark red-brown solutions. The complex has been characterized by single-crystal X-ray diffraction, variable-temperature ^{119}Sn, ^{31}P, ^{195}Pt NMR spectroscopy, electrospray mass spectrometry (ESI-MS), and elemental analysis.

En solutions of K_4Sn_9 also react with toluene solutions of $Ni(CO)_2(PPh_3)_2$ in the presence of 2,2,2-cryptand to give low but reproducible yields of the $[Sn_9Ni_2(CO)]^{3-}$ ion (**3**) as the $[K(2,2,2\text{-crypt})]^+$ salt. The reaction is complicated by the competitive formation of Sn_9^{3-} and $[Ni_2(CO)_2(PPh_3)_2(\mu\text{-}CO)(\mu\text{-}PPh_2)]^{1-}$ (see ref 32) although the formation of **3** presumably follows a similar pathway (eq 3). The $[K(2,2,2\text{-crypt})]_3[Sn_9Ni_2(CO)]$ salt is air sensitive in the solid state and in solution and is soluble in DMF. The complex is paramagnetic and has been characterized by EPR and IR spectroscopy, ESI-MS, and single-crystal X-ray diffraction.

$$\underset{(\mathbf{1})}{Sn_9^{4-}} + 2Ni(CO)_2(PPh_3)_2 + en \xrightarrow{(2,2,2-crypt)} \underset{(\mathbf{3})}{[Sn_9Ni_2(CO)]^{3-}} + 4PPh_3 + 3CO + [H_2N(CH_2)_2NH]^{1-} + {}^1/_2H_2 \quad (3)$$

Solid-State Structures. The $[K(2,2,2\text{-crypt})]_2[Sn_9Pt_2(PPh_3)]$ salt crystallizes in two different triclinic polymorphs: one with an ethylenediamine solvate molecule and one with a toluene solvate molecule in the crystal lattice. Summaries of the crystallographic data for both polymorphs are found in Table 1. The $[Sn_9Pt_2(PPh_3)]^{2-}$ ion is slightly disordered in both polymorphs, and one arm of one $[K(2,2,2\text{-crypt})]^+$ ion is slightly disordered in the toluene solvate polymorph. The structures are otherwise identical. Selected bond distances for the en solvate structure are given in Table 2. Two views of the $[Sn_9Pt_2(PPh_3)]^{2-}$ ion are shown in Figure 1.

The $[Sn_9Pt_2(PPh_3)]^{2-}$ ion has virtual C_{3v} point symmetry defined by an elongated tricapped trigonal prismatic Sn_9 cluster with a linear Pt−Pt−PPh_3 rod inserted into the top triangular face. The Sn_9 group of the $[Sn_9Pt_2(PPh_3)]^{2-}$ ion can be viewed as a derivative of a *closo*-Sn_9^{2-} ion which has D_{3h} point symmetry (see **II**). In that ion and the known *closo*-Sn_9^{3-} ion, the clusters adopt regular tricapped trigonal prismatic structures with Sn−Sn bond distances in the range 2.926−3.315 Å. In $[Sn_9Pt_2(PPh_3)]^{2-}$, the three longitudinal Sn−Sn contacts of the trigonal prism (see h, drawing **II**) are elongated to 3.57 Å (av), which can be considered nonbonding, and the three bonds of the top triangular face of Sn_9^{3-} (see t, drawing **II**) are broken with Sn−Sn separations of 4.02 Å (av). Finally, the $Pt_2(PPh_3)$ unit is inserted into the top face to form the $[Sn_9Pt_2(PPh_3)]^{2-}$ cluster (see **III**). The Sn−Sn bonds that remain in $[Sn_9Pt_2(PPh_3)]^{2-}$ are in the range 3.002(2) − 3.136(3) Å. For comparison, there are 15 contacts under 3.32 Å in $[Sn_9Pt_2(PPh_3)]^{2-}$ versus 20 such contacts for *nido*-Sn_9^{4-} and [*closo*-Sn_9M-

(17) Eichhorn, B. W.; Haushalter, R. C.; Pennington, W. T. *J. Am. Chem. Soc.* **1988**, *110*, 8704.
(18) Campbell, J.; Mercier, H. P. A.; Holger, F.; Santry, D.; Dixon, D. A.; Schrobilgen, G. J. *Inorg. Chem.* **2002**, *41*, 86.
(19) Schiemenz, B.; Huttner, G. *Angew. Chem., Int. Ed. Engl.* **1993**, *32*, 297.
(20) Renner, G.; Kircher, P.; Huttner, G.; Rutsch, P.; Heinze, K. *Eur. J. Inorg. Chem.* **2001**, 973.
(21) Kesanli, B.; Eichhorn, B. W.; Fettinger, J. C. *Angew. Chem., Int. Ed.* **2001**, *40*, 2300.
(22) Teixidor, F.; Leutkens, M. L., Jr.; Rudolph, R. W. *J. Am. Chem. Soc.* **1983**, *105*, 149.
(23) Kesanli, B.; Charles, S.; Lam, Y.-F.; Fettinger, J. C.; Eichhorn, B. W. *J. Am. Chem. Soc.* **2000**, *122*, 11101.

Table 1. Crystallographic Data for the $[Sn_9Pt_2(PPh_3)]^{2-}$ and $[Sn_9Ni_2(CO)]^{3-}$ Ions

empirical formula	$C_{56}H_{95}K_2N_6O_{12}PPt_2Sn_9$	$C_{61}H_{95}K_2N_4O_{12}PPt_2Sn_9$	$C_{132}H_{247}K_6N_8Ni_4O_{38}PSn_{18}$
compound formula	$[K(crypt)]_2$**2**·en	$[K(crypt)]_2$**2**·tol	$[K(crypt)]_6$**3**$_2$·2en·$^1/_2$ PPh_3
formula weight	2611.94	2643.97	21213.15
temperature (K)	193(2)	293(2)	293(2)
wavelength (Å)	0.710 73	0.710 73	0.710 73
crystal system	triclinic	triclinic	monoclinic
space group	$P\bar{1}$	$P\bar{1}$	$P2_1/c$
unit cell dimensions			
a (Å)	13.1703(6)	12.4953(16)	31.1970(10)
b (Å)	13.3120(6)	13.7484(18)	23.8741(8)
c (Å)	24.3236(10)	24.276(3)	27.9617(9)
α (deg)	79.4450(10)	86.795(2)	90
β (deg)	76.0670(10)	86.925(2)	113.0470(10)
γ (deg)	83.7260(10)	83.240(2)	90
volume (Å^3)	4059.5(3)	4130.2(9)	19163.6(11)
Z	2	2	4
D_{calc} (g/cm^3)	2.137	2.126	1.838
abs coeff (mm^{-1})	6.322	6.214	2.884
crystal size (mm)	0.105 × 0.083 × 0.040	0.364 × 0.310 × 0.205	0.521 × 0.312 × 0.026
index ranges	$-15\le h\le 15$, $-15\le k\le 15$, $-28\le l\le 28$	$-14\le h\le 14$, $-16\le k\le 16$, $-28\le l\le 28$	$-37\le h\le 37$, $-28\le k\le 28$, $-33\le l\le 33$
reflections collected	53 909	28 663	124 417
independent reflections	14 288 [R(int) = 0.0595]	14 508 [R(int) = 0.0399]	33 750 [R(int) = 0.0477]
data/restraints/parameters	14 288/0/875	14 508/0/889	33 750/37/2081
goodness of fit on F^2	1.012	1.032	1.059
final R indices [$I > 2\sigma(I)$][a]			
R1	0.0398	0.0579	0.0513
wR2	0.0684 (9417 data)	0.1830 (11 098 data)	0.1403 (22 547 data)
R indices (all data)			
R1	0.0790	0.0781	0.0849
wR2	0.0819	0.1930	0.1558
extinction coefficient	0.000 036(11)	N/R[b]	N/R[b]
largest peak/hole (e·Å^{-3})	0.858 and −1.078	2.940 and −1.403	2.567 and −1.365

[a] The function minimized during the full-matrix least-squares refinement was $\sum w(F_o2 - F_c^2)$, where $w=1/[\sigma^2(F_o^2) + (0.0180P)^2 + 10.4114P]$ and $P = (\max(F_o^2,0) + 2F_c^2)/3$. [b] Not refined.

Table 2. Selected Bond Lengths (Å) for $[Sn_9Pt_2(PPh_3)]^{2-}$

Pt(1)−P(1)	2.214(2)	Sn(2)−Sn(4)	3.002(2)
Pt(1)−Sn(3)	2.6735(13)	Sn(2)−Sn(5)	3.004(3)
Pt(1)−Sn(2)	2.6867(15)	Sn(3)−Sn(6)	3.002(2)
Pt(1)−Pt(2)	2.6965(4)	Sn(3)−Sn(4)	3.018(2)
Pt(1)−Sn(1)	2.714(3)	Sn(4)−Sn(7)	3.088(3)
Pt(2)−Sn(2)	2.6749(16)	Sn(4)−Sn(9)	3.125(3)
Pt(2)−Sn(1)	2.686(3)	Sn(5)−Sn(8)	3.091(4)
Pt(2)−Sn(3)	2.689(2)	Sn(5)−Sn(9)	3.136(3)
P(1)−C(1)	1.829(8)	Sn(6)−Sn(7)	3.100(3)
P(1)−C(7)	1.829(7)	Sn(6)−Sn(8)	3.132(3)
P(1)−C(13)	1.842(8)	Sn(7)−Sn(9)	3.008(4)
Sn(1)−Sn(6)	3.007(3)	Sn(7)−Sn(8)	3.046(3)
Sn(1)−Sn(5)	3.009(3)	Sn(8)−Sn(9)	3.046(4)

$(CO)_3]^{4-}$[16,17] and 21 in the *closo*-Sn_9^{3-} ions.[2] As such, the Sn_9 cluster in the $[Sn_9Pt_2(PPh_3)]^{2-}$ ion is at best a highly distorted variant of the deltahedral Sn_9 family.

The Pt(2) atom resides in the center of the tricapped trigonal prismatic Sn_9 cluster with nine Pt−Sn contacts in a narrow range of 2.675(3)−2.793(2) Å. Pt(1) caps the top of the triangular face of the cluster with three Pt−Sn bonds of 2.69(2) Å (av). The PPh_3 ligand is also coordinated to Pt(1), which completes its pseudotetrahedral coordination sphere. The Pt(1)−Pt(2) distance (2.6965(4) Å) is indicative of direct Pt−Pt bonding,[24,25] which is consistent with the spectroscopic properties of the ion (see NMR section).

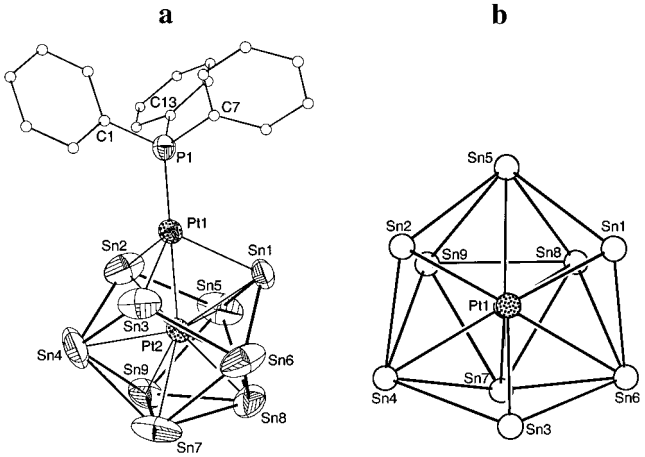

Figure 1. Two views of the $[Sn_9Pt_2(PPh_3)]^{2-}$ ion, **2**, showing (a) side view and (b) top view down the P−Pt−Pt axis. The PPh_3 ligand is omitted in (b) for clarity.

The $[K(2,2,2\text{-crypt})]^+$ salt of $[Sn_9Ni_2(CO)]^{3-}$ is monoclinic, space group $P2_1/c$, and contains two independent $[Sn_9Ni_2(CO)]^{3-}$ clusters, six $[K(2,2,2\text{-crypt})]^+$ ions, two en molecules, and a free PPh_3 molecule in the asymmetric unit. Both of the $[Sn_9Ni_2(CO)]^{3-}$ "sites" show disorder such that there are two different orientations of the anion on each single site with relative occupancies 85:15 (see crystallography in the Experimental Section and Supporting Information). The disorder on both sites was successfully modeled, and the four independent anions are the same (within experimental error). The only structural feature that significantly differs between the two

(24) Reinartz, S.; Baik, M.-H.; White, P. S.; Brookhart, M.; Templeton, J. L. *Inorg. Chem.* **2001**, *40*, 4726.
(25) Tanase, T.; Ukaji, H.; Takahata, H.; Toda, H.; Igoshi, T.; Yamamoto, Y. *Organometallics* **1998**, *17*, 196.

Table 3. Bond Lengths [Å] for $[Sn_9Ni_2(CO)]^{3-}$

Ni(1)−C(1)	1.596(14)	Sn(1)−Sn(2)	3.0300(8)
Ni(1)−Ni(2)	2.656(6)	Sn(1)−Sn(5)	3.240(4)
Ni(1)−Sn(5)	2.683(8)	Sn(2)−Sn(9)	2.8268(12)
Ni(1)−Sn(4	2.683(5)	Sn(2)−Sn(3)	3.005(2)
Ni(1)−Sn(3)	2.710(7)	Sn(3)−Sn(6)	3.036(4)
Ni(1)−Sn(1)	2.753(6)	Sn(3)−Sn(4)	3.253(5)
O(1)−C(1)	1.181(13)	Sn(4)−Sn(6)	2.988(5)
Ni(2)−Sn(4)	2.619(4)	Sn(4)−Sn(7)	2.998(5)
Ni(2)−Sn(2)	2.6242(10)	Sn(4)−Sn(5)	3.250(5)
Ni(2)−Sn(7)	2.625(3)	Sn(5)−Sn(7)	3.016(6)
Ni(2)−Sn(5)	2.625(4)	Sn(5)−Sn(8)	3.080(5)
Ni(2)−Sn(1)	2.6310(9)	Sn(6)−Sn(9)	2.870(4)
Ni(2)−Sn(3)	2.637(3)	Sn(7)−Sn(9)	2.930(4)
Sn(1)−Sn(8)	2.988(3)	Sn(8)−Sn(9)	2.918(2)

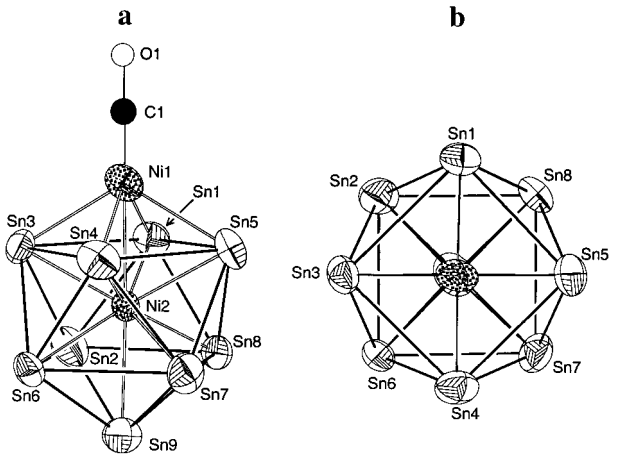

Figure 2. Two ORTEP drawings of the $[Sn_9Ni_2(CO)]^{3-}$ ion, **3**, showing (a) side view and (b) top view down the O−C−Ni−Ni−Sn9 axis (CO ligand omitted in (b) for clairty).

clusters is the Ni−Ni separation, 2.534(3) Å in one and 2.656(6) Å in the other, which is presumably an artifact of the disorder. The type of disorder is somewhat different on the two sites, and only the major orientation from one of the sites is presented here. A summary of the crystallographic data is given in Table 1, and selected bond distances for the $[Sn_9Ni_2(CO)]^{3-}$ ion are given in Table 3. Two views of the $[Sn_9Ni_2(CO)]^{3-}$ ion are given in Figure 2.

The $[Sn_9Ni_2(CO)]^{3-}$ anion possesses a fairly regular *closo*-10-vertex Sn_9Ni framework with an additional interstitial Ni atom, Ni(2). The complex possesses virtual C_{4v} point symmetry with a relatively unperturbed Sn_9 fragment. Aside from the interstitial atom, the structure is quite similar to that of [*closo*-$Sn_9M(CO)_3]^{4-}$ ions where M = Cr, Mo, W.[16,17] According to Wade's rules,[13,26] the $[Sn_9Ni_2(CO)]^{3-}$ cluster is a 10-vertex 21-electron polyhedron, which is consistent with the observed *closo* geometry. The framework Ni atom, Ni(1), caps the open square face of the parent *nido*-Sn_9^{4-} cluster and has an additional carbonyl ligand that occupies the apical position in a square pyramidal coordination sphere. The four Ni(1)−Sn contacts average 2.71(2) Å whereas the Ni−C distance is 1.60(2) Å. There is a ∼0.2 Å elongation of the Sn−Sn contacts around the top belt relative to the [*closo*-$Sn_9M(CO)_3]^{4-}$ structures and *nido*-Sn_9^{4-}; however, the remainder of the cluster is quite similar. The 20 Sn−Sn bonding contacts in $[Sn_9Ni_2(CO)]^{3-}$ are in the range 2.827(3)−3.383(2) Å, which are similar to those

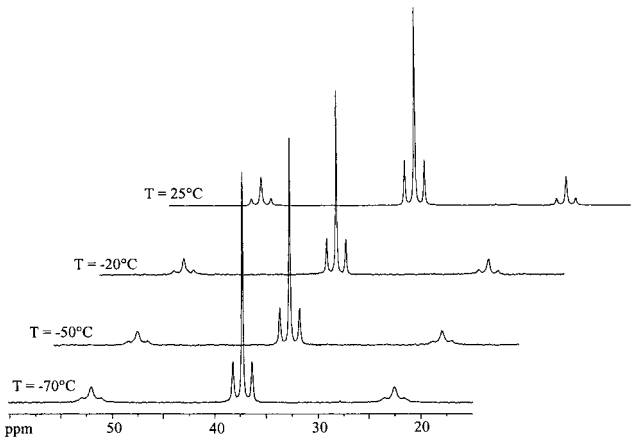

Figure 3. Variable-temperature ^{31}P NMR spectra for the $[Sn_9Pt_2(PPh_3)]^{2-}$ ion, **2**. Data were recorded at 162 MHz from a DMF solution. For clarity, the stacked spectra are offset to the right.

in the [*closo*-$Sn_9M(CO)_3]^{4-}$ structures and *nido*-Sn_9^{4-}. The interstitial Ni atom resides in a Sn_9Ni bicapped square antiprismatic hole with Sn−Ni distances in the narrow range of 2.619(4)−2.681(2) Å.

NMR and EPR Spectroscopic Studies. (1) $[Sn_9Pt_2(PPh_3)]^{2-}$. The variable-temperature ^{31}P NMR spectra for $[Sn_9Pt_2(PPh_3)]^{2-}$ are shown in Figure 3. The room-temperature spectrum is consistent with the solid-state structure showing a single resonance flanked by two sets of Pt satellites (^{195}Pt, $I = {}^1/_2$, 33.7% abundance) with coupling constants $^1J_{^{195}Pt-^{31}P} = 4800$ Hz and $^2J_{^{195}Pt-^{31}P} = 305$ Hz. As the temperature is lowered, the outer satellites broaden whereas the inner satellites and the central resonance remain sharp. Because the phosphine ligand does not dissociate (Pt−P coupling is maintained at room temperature) and cannot be in dynamic exchange (there is only one PPh_3 ligand), the broadening is most likely due to tumbling effects associated with chemical shift anisotropy.[27] Note that P−Sn coupling is not resolved. The ^{31}P NMR data show that: (1) the Pt−Pt−PPh_3 unit remains intact and (2) the two Pt atoms are not in exchange on the NMR time scale (two distinct sets of satellites).

In contrast, the ^{119}Sn spectrum of $[Sn_9Pt_2(PPh_3)]^{2-}$ reveals dynamic behavior. The complex shows a single ^{119}Sn resonance with a lone set of ^{195}Pt satellites ($^1J_{^{195}Pt-^{119}Sn} = 1690$ Hz) due to coupling to the interstitial Pt atom (see Figure 4). This assignment is based on the ^{195}Pt NMR spectrum and is discussed below. Importantly, the ^{119}Sn spectrum is inconsistent with the solid-state structure (three equal intensity resonances expected) and does not show coupling to the vertex Pt atom or any ^{117}Sn satellites (^{119}Sn, $I = {}^1/_2$, 8.7% abundance; ^{117}Sn, $I = {}^1/_2$, 7.7% abundance). Upon cooling, the resonance broadens into the baseline but does not reemerge at −72 °C (DMF/tol, 149 MHz). These data are indicative of a highly fluxional Sn_9 cluster with a rigid Pt_2PPh_3 fragment. The ^{195}Pt NMR data support this conclusion showing two resonances ($\delta = -5270$ and -6010 ppm) arising from the interstitial and vertex Pt atoms, respectively (see Figure 5). Both resonances show Pt satellites due to the one-bond Pt−Pt coupling of 2472 Hz. The peaks are easily assigned from the ^{31}P couplings of 305 and 4800 Hz associated with the interstitial ($\delta = -5270$) and vertex ($\delta = -6010$)

(26) *Electron Deficient Boron and Carbon Clusters*; Olah, G. A., Wade, K., Williams, R. E., Eds.; Wiley: New York, 1991; p 11.

(27) Bovey, F. A. *Nuclear Magnetic Resonance Spectroscopy*, 2nd ed.; Academic Press: San Diego, CA, 1988.

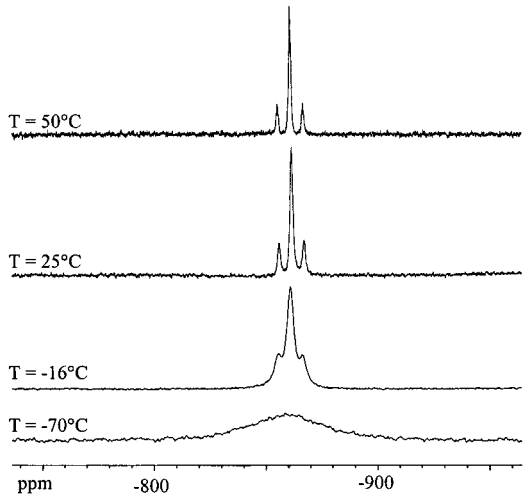

Figure 4. Variable-temperature ^{119}Sn NMR spectra for the $[Sn_9Pt_2(PPh_3)]^{2-}$ ion, **2**. Data were recorded at 186.5 MHz from a DMF solution.

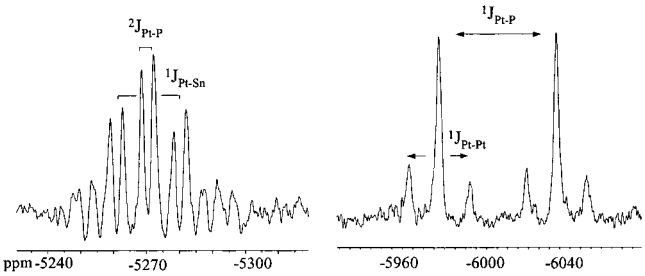

Figure 5. ^{195}Pt NMR spectra for the $[Sn_9Pt_2(PPh_3)]^{2-}$ ion, **2**. Data were recorded at 85.5 MHz and −10 °C from a DMF solution.

Pt atoms, respectively. Interestingly, only the interstitial Pt resonance shows tin satellites ($^1J_{^{195}Pt-^{119/117}Sn} \approx 1690$ Hz), which is consistent with the single set of ^{195}Pt satellites on the ^{119}Sn resonance. The Sn−Pt coupling to the vertex Pt atom is too small to resolve.

The NMR data paint a consistent picture of an unusual fluxional process associated with the $[Sn_9Pt_2(PPh_3)]^{2-}$ ion. The dynamic behavior involves rapid exchange of all nine Sn atoms about a static Pt−Pt−PPh_3 fragment. The large Pt−Sn coupling associated with the interstitial Pt resonance indicates that the Sn−Pt(2) interactions remain strong throughout the exchange process. The lack of Pt−Sn coupling to the vertex Pt atom (or its small value) is due to the averaging of the expected large couplings to Sn(1,2,3) (i.e., $^1J_{^{195}Pt-^{119/117}Sn} \approx 1690$ Hz) and small couplings ($^{2,3}J_{^{195}Pt-^{119/117}Sn} \approx 0$ Hz) predicted from the solid-state structure. Although Sn−Pt coupling to the vertex Pt atom is not detected, it is clear that the exchange is intramolecular and the vertex Pt−PPh_3 fragment is not dissociating from the Sn_9 center. The maintenance of the strong $^1J_{^{195}Pt-^{195}Pt}$ coupling and $^2J_{^{195}Pt-^{31}P}$ coupling during the exchange process verifies this conclusion. The dynamic behavior can be viewed as a liquidlike Sn_9 matrix surrounding a rigid Pt−Pt−PPh_3 stick.

(2) $[Sn_9Ni_2(CO)]^{3-}$. The EPR spectrum of $[Sn_9Ni_2(CO)]^{3-}$ (Figure 6) shows a hyperfine of 4.8 G due to interactions with the nine tin atoms of the cluster (^{119}Sn, $I = {}^1/_2$, 8.7% abundance; ^{117}Sn, $I = {}^1/_2$, 7.7% abundance). The best simulations (peak intensity matches) are obtained when all nine tin atoms are included as contributing nuclei (see inset of Figure 6). However, the small high-frequency lines obtained from these models are not observed in the experimental spectrum. These peaks are

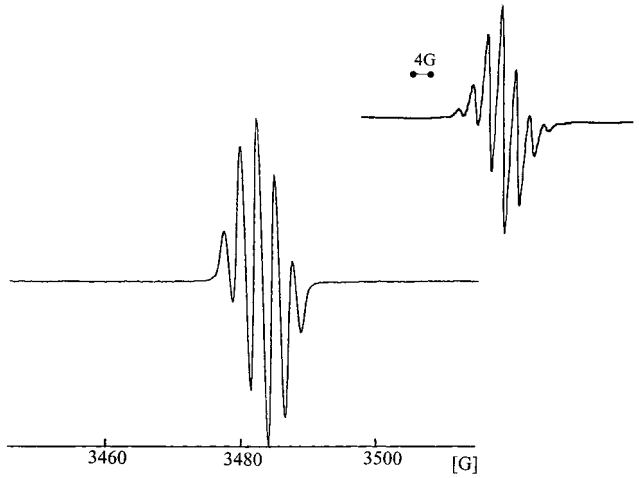

Figure 6. EPR spectrum for the $[Sn_9Ni_2(CO)]^{3-}$ ion, **3**, recorded from DMF solution at 25 °C. The simulated spectrum is shown in inset.

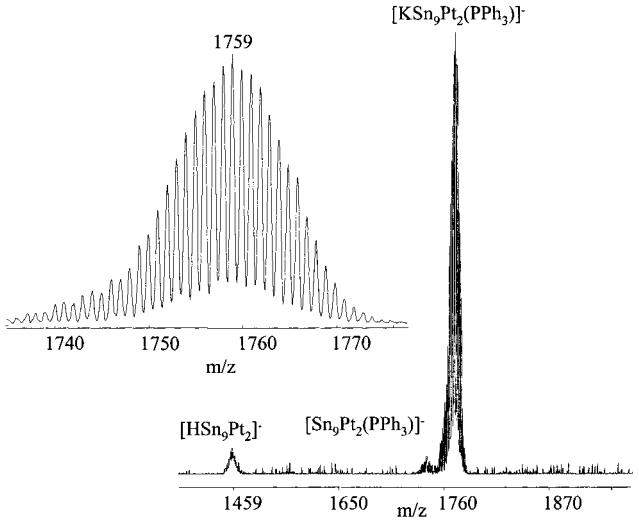

Figure 7. Electrospray mass spectrum (negative ion mode) of $[Sn_9Pt_2(PPh_3)]^{2-}$ recorded from a DMF solution.

presumable lost due to broadening effects associated with the slow tumbling of the cluster.[28] The IR spectrum of the cluster (KBr pellet) shows a CO stretch at 1851 cm^{-1}.

Electrospray Mass Spectrometry. The electrospray mass spectrum (negative ion mode) recorded from a DMF solution of crystalline $[K(2,2,2\text{-crypt})]_2[Sn_9Pt_2(PPh_3)]$ is shown in Figure 7. As is common for these types of Zintl ions,[7,29−31] the $[Sn_9Pt_2(PPh_3)]^{2-}$ molecular ion is not observed. Instead, the potassium-coordinated ion pair, $K[Sn_9Pt_2(PPh_3)]^{1-}$, appears as the parent ion with a spectacular mass envelope arising from the multiple isotopes of Sn and Pt. Fassler et al. found similar results with the naked group 14 cluster anions.[7] The two other prominent ions are the oxidized molecular ion, $[Sn_9Pt_2(PPh_3)]^{1-}$, and the ligand-free protonated binary ion, $[HSn_9Pt_2]^{1-}$.

The electrospray mass spectrum of $[K(2,2,2\text{-crypt})]_3[Sn_9Ni_2(CO)]$, recorded from a DMF solution, is more complicated, showing various decomposition species and presumably impuri-

(28) Wertz, J. E.; Bolton, J. R. *Electron Spin Resonance. Elementary Theory and Practical Applications*; Chapman and Hall: New York, 1986.
(29) Moses, M.; Fettinger, J. C.; Eichhorn, B. W. *J. Am. Chem. Soc.*, in press.
(30) Kesanli, B.; Fettinger, J. C.; Eichhorn, B. W., results to be published.
(31) Eichhorn, B. W.; Matamanna, S. P.; Gardner, D. R.; Fettinger, J. C. *J. Am. Chem. Soc.* **1998**, *120*, 9708.

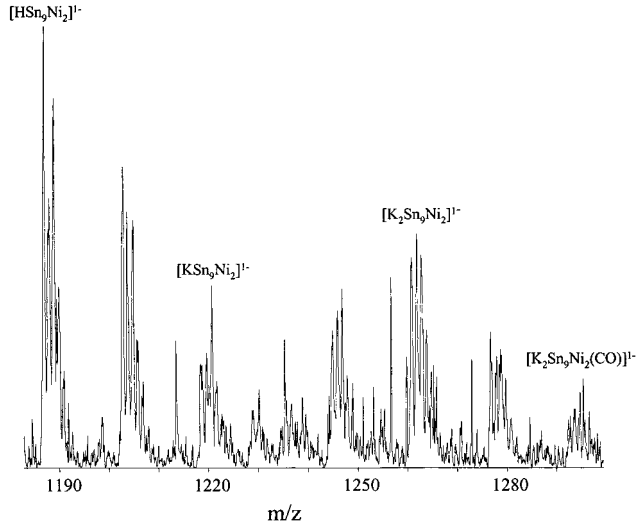

Figure 8. Electrospray mass spectrum (negative ion mode) of $[Sn_9Ni_2(CO)]^{3-}$ recorded from a DMF solution.

ties that cocrystallize with the title compound[32] (e.g., Sn_9^{3-}; see Synthesis section). Weak signals for the potassium complex, $[K_2Sn_9Ni_2(CO)]^{1-}$, as well as the ligand-free binary ions $[K_2Sn_9Ni_2]^{1-}$, $[KSn_9Ni_2]^{1-}$, and $[HSn_9Ni_2]^{1-}$ were observed (see Figure 8).

Discussion

The synthesis of the $[Sn_9Pt_2(PPh_3)]^{2-}$ ion, **2**, follows a complicated, multistep pathway involving at least one intermediate. Although the details of the reaction mechanism are not know, the data are consistent with the double solvent-activation process outlined in eq 1. The formation of H_2 in eq 1 could, in theory, occur by way of a double protonation and H_2 elimination reaction in which the protons originate from impurities in the solvent. However, deuterium labeling studies using DMSO-d_6 as the solvent in eq 1 gives D_2, which again is indicative of the double hydrogen atom abstraction process outlined in eq 1. Similar labeling studies in the closely related $[P_7PtH(PPh_3)]^{2-}$ chemistry[23] also showed that the hydride ligand originated from the activation of solvent molecules and not from impurities. The fact that a two-electron oxidation has occurred in the Sn−Pt system versus a one-electron oxidation in the P−Pt system is consistent with the enhanced donor abilities of the Sn_9^{4-} ligand relative to the P_7^{3-} ligand. Moreover, the one-electron oxidation in the Ni−Sn system to give $[Sn_9Ni_2(CO)]^{3-}$ (**3**) instead of a two-electron oxidiation analogue of **2** (i.e., $[Sn_9Ni_2(CO)]^{2-}$) is also consistent with the lower reducing capacity of Ni relative to Pt. The presence of an electron-withdrawing CO ligand relative to the electron-donating ligand PPh_3 may also contribute to the differences in oxidation states. For example, the same one-electron difference in cluster oxidation was observed in the chemistry of P_7^{3-} in reactions with the same $Ni(CO)_2(PPh_3)_2$ and $Pt(PPh_3)_4$ precursors used in the present study. The observed products from those reactions, $[P_7Ni(CO)]^{3-}$ and $[P_7PtH(PPh_3)]^{2-}$, result from a simple non-oxidative insertion and a single solvent activation process, respectively.[23,33]

In the solid state, **3** adopts a *closo*-type architecture that is consistent with its 10-vertex 21-electron count. The structure is quite similar to that of the $[Sn_9M(CO)_3]^{4-}$ ions (10-vertex, 22-electrons)[16−18] with only a minor expansion of the top belt, which presumably arises from the incorporation of the Ni interstitial. In contrast, **2** adopts a nondeltahedral structure despite its *hypercloso* 10-vertex 20-electron configuration. Although the Sn_9 fragment of **2** is a derivative of the *closo*-Sn_9^{2-} structure, the incorporation of the Pt_2PPh_3 unit ruptures six of the bonds in the Sn_9 fragment to generate a new type of C_{3v} framework (see **II** and **III**). The striking differences between **2** and **3**, despite their similarities in composition and electron count, may be due to the difference in metal−metal distances of the two M_2L fragments. It is possible that the required Pt−Pt separation is too long for the C_{4v} structure type, and the highly distorted C_{3v} structure of **2** may reflect the optimization of Pt−Sn and Pt−Pt bonds at the expense of Sn−Sn bonding. Unfortunately, the variation of the Ni−Ni separations in **3** due to disorder precludes a quantitative assessment of these metric parameters.

Perhaps the most interesting features of **2** and **3** are their spectroscopic/dynamic properties. In particular, the dynamic behavior of $[Sn_9Pt_2(PPh_3)]^{2-}$ is similar to that of Sn_9^{4-} showing global exchange of all nine Sn atoms. This behavior contrasts that of the static Sn_6 clusters, *closo*-$\{[Sn_6[Cr(CO)_5]_6\}^{2-}$,[19,20] and $[(\eta\text{-}C_7H_8)Nb(cyclo\text{-}Sn_6)Nb(\eta\text{-}C_7H_8)]^{2-}$,[21] as well as the local exchange that occurs in the *closo*-$[Sn_9M(CO)_3]^{4-}$ ions.[16] The highly distorted nature of the C_{3v} structure of **2** and the low coordination numbers of the Sn atoms in the Sn_9 cage presumably leave the Sn atoms in an unstable situation where other structures (e.g., the *closo*-C_{4v} structure) are close in energy. Rapid interconversion of these structure types could account for the exchange of the Sn sites. Moreover, a $C_{3v} \rightleftharpoons C_{4v}$ equilibrium would account for the nonexchange of the Pt sites as well as the retention of the Pt−Pt and Sn−$Pt_{interstitial}$ couplings.

The dynamic behavior of $[Sn_9Ni_2(CO)]^{3-}$ is more difficult to assess due to the paramagnetic behavior of the compound. The local $\eta^4 \rightleftharpoons \eta^5$ exchange observed for the closely related *closo*-$[Sn_9M(CO)_3]^{4-}$ ions may be operative in **3** as well, but a diamagnetic derivative is needed to study this system. It is interesting to note that **3** gives a sharp EPR spectrum with well-defined Sn hyperfine in solution, as expected, whereas the solution EPR spectra for the paramagnetic E_9^{3-} ions (E = Ge, Sn, Pb) show either no signals or broad signals with no discernible hyperfine.[3] Sharp EPR signals and hyperfine main-group couplings in the paramagnetic *cyclo*-E_8M^{n-} ions (E = As, Sb, M = Cr, Mo)[30] are also observed. These studies show that paramagnetic Zintl ions can be prepared and isolated but a transition metal may be necessary to stabilize the complex.

Finally, it is important to note that the $HSn_9Ni_2^{1-}$ and $HSn_9Pt_2^{1-}$ ions observed in the mass spectrometry studies represent a growing class of naked binary cluster anions. While these complexes may not be isolable, others such as $Sn_{18}Pt_2^{4-}$, the *cyclo*-E_8M^{n-} ions (E = As, Sb, M = Cr, Mo, Nb),[30,31] $[As_{14}Pd_2]^{4-}$, and $[As_{16}Pd_7]^{4-}$ are quite stable[29] and have been fully characterized. Unlike other binary systems, such as the metcars[34−36] and the gas-phase metal−As systems,[37] we have

(32) Kesanli, B.; Gardner, D. R.; Scott, B.; Eichhorn, B. W. *J. Chem. Soc., Dalton Trans.* **2000**, 1291.
(33) Charles, S.; Eichhorn, B. W.; Bott, S. G.; Fettinger, J. C. *J. Am. Chem. Soc.* **1996**, *118*, 4713.
(34) Deng, H. T.; Kerns, K. P.; Castleman, A. W. J. *J. Am. Chem. Soc.* **1996**, *118*, 446.

direct knowledge of structure and dynamics of these clusters and can monitor their transformations into metastable solids and nanoparticles.

Experimental Section

General Data. All reactions were performed in a nitrogen-filled drybox (Vacuum Atmospheres Co.). $^{31}P\{^1H\}$ NMR, ^{119}Sn NMR, and ^{195}Pt NMR spectra were recorded on a Bruker AM400 Avance spectrometer operating at 162, 149, and 85.5 MHz, respectively. The $^{31}P\{^1H\}$ NMR data were referenced against an external 85% H_3PO_4/CD_2Cl_2 standard (0 ppm). ^{119}Sn chemical shift was referenced to Me_4Sn in C_6D_6 (0 ppm). An aqueous solution of $[PtCl_6]^{2-}$ (0 ppm) was used for the ^{195}Pt NMR experiments. Delays of 0.5 s were used in all pulse sequences except the ^{195}Pt NMR experiments, which required delay times of 1 s. DMF-d_7/tol-d_8 mixtures were used as an internal lock for low-temperature studies. Block searches of 500 and 800 ppm windows were used in the exploratory ^{119}Sn and ^{195}Pt NMR analyses, respectively. A Bruker 200D-SRC EPR spectrometer was used for the EPR analysis. Samples were drawn into 50-μL capillaries in a drybox and sealed at the top and bottom. The sealed capillaries were then placed within standard 3-mm-internal diameter quartz EPR tubes. Electrospray mass spectra were recorded from DMF solutions on a Finnigan mass spectrometer by way of direct injection. The samples were ionized by using an ESI probe and detected in the negative ion mode. IR spectra were recorded from KBr pellets on a Nicolet 560 FTIR spectrometer. Elemental analyses were performed under inert atmospheres by Atlantic Microlab, Inc. (Norcross, GA).

Chemicals. K_4Sn_9 was prepared by high-temperature fusion (~1000 °C) of stoichiometric ratios of the elements. The chemicals were sealed in evacuated, silica tubes and carefully heated with a natural gas/oxygen flame. ***Caution:*** *molten alloy synthesis can result in serious explosion and reactions should be conducted with great caution behind blast shields*. 4,7,13,16,21,24-Hexaoxa-1,10-diazobicyclo[8.8.8]hexacosane (2,2,2-crypt), Pd (10%) on carbon, *trans*-stilbene, and $Ni(CO)_2(PPh_3)_2$ were purchased from Aldrich. $Pt(PPh_3)_4$ was purchased from Strem. Anhydrous ethylenediamine (en) and dimethylformamide (DMF) were purchased from Fisher, vacuum distilled from K_4Sn_9, and stored under dinitrogen. Toluene was distilled from sodium/benzophenone under dinitrogen and stored under dinitrogen.

Synthesis. (1) Preparation of $[K(2,2,2\text{-crypt})]_2[Sn_9Pt_2(PPh_3)]\cdot$tol. In vial 1, K_4Sn_9 (80 mg, 0.065 mmol) was dissolved in en (~2 mL) producing a red solution. In vial 2, $Pt(PPh_3)_4$ (80 mg, 0.065 mmol) was dissolved in toluene (~2 mL) producing a yellow solution. The contents of vial 2 were added to the contents of vial 1, 4 equivalents of crypt (98 mg, 0.26 mmol) were added as a solid, and the reaction mixture was stirred for 2 h yielding a dark red-brown solution. The reaction mixture was filtered through tightly packed glass wool in a pipet. Dark red crystals formed in the reaction vessel after 24 h (25 mg, 29%). $^{31}P\{^1H\}$NMR (DMF-d_7/tol-d_8, 25 °C): δ (ppm) 35.4 ($^1J_{Pt-P}$ = 4800 Hz; $^2J_{Pt-P}$ = 305 Hz).^{119}Sn NMR (DMF-d_7/tol-d_8): δ (ppm) −862 ($^1J_{Pt-Sn}$ = 1690 Hz). ^{195}Pt NMR (DMF-d_7/tol-d_8): δ (ppm) −5270 ($^2J_{Pt-P}$ = 305 Hz; $^1J_{Pt-Sn}$ = 1690 Hz), −6010 ($^1J_{Pt-P}$ = 4800; $^1J_{Pt-Pt}$ = 2472 Hz). Anal. Calcd for $K_2Sn_9Pt_2PC_{61}H_{95}O_{12}N_4$: C, 27.7; H, 3.6; N, 2.1. Found: C, 27.2; H, 3.7; N, 2.5. The en solvate complex, $[K(2,2,2\text{-crypt})]_2[Sn_9Pt_2(PPh_3)]\cdot$en, forms under identical conditions.

(2) Preparation of $[K(2,2,2\text{-crypt})]_3[Sn_9Ni_2(CO)]\cdot$en$\cdot(PPh_3)_{0.5}$. In vial 1, K_4Sn_9 (60 mg, 0.049 mmol) was dissolved in en (~2 mL) producing a red solution. In vial 2, $Ni(CO)_2(PPh_3)_2$ (31 mg, 0.049 mmol) was dissolved in toluene (~2 mL) and gently heated to give a yellow solution. The contents of vial 2 were added to the contents of vial 1 and 4 equiv of crypt (74 mg, 0.20 mmol) were added as a solid. The reaction mixture was stirred for 2 h, yielding a dark red-brown solution. It was then filtered through tightly packed glass wool in a pipet. Black crystals formed in the reaction vessel after 3 days. IR (KBr pellet): 1851 cm^{-1} (ν_{CO}).

(3) Hydrogenation of *trans*-Stilbene. (A) K_4Sn_9 (160 mg, 0.13 mmol), $Pt(PPh_3)_4$ (160 mg, 0.13 mmol), and 4 equiv of crypt (195 mg, 0.52 mmol) were weighed into a 50-mL flask. A small vial (no top) containing *trans*-stilbene (5 mg, 0.026 mmol) and 0.1 equiv Pd/C catalyst suspended in hexane (~3 mL) was set inside the flask containing the solids. An en/tol solvent mixture (~10 mL) was introduced into the flask via syringe. The reaction flask was capped tightly, and the mixtures were stirred for 12 h. The contents of the inner vial were filtered through tightly packed glass wool in a pipet and evaporated to dryness in vacuo. ^1H NMR spectroscopic analysis of the white solid showed the formation of bibenzyl (~90% conversion). (B) A procedure identical to that described above was used except a tol/DMSO-d_6 solvent mixture was used in the flask and tol was used instead of hexane in the vial. ^1H NMR spectroscopic analysis of the white solid showed the formation of bibenzyl-d_2 (~90% conversion) as the only hydrogenation product. Identical experiments using protonated DMSO and tol-d_8 gave only protonated bibenzyl.

Crystallographic Studies. (1) $[K(2,2,2\text{-crypt})]_2[Sn_9Pt_2(PPh_3)]\cdot$en. A dark red block was placed and optically centered on the Bruker SMART CCD system at −80 °C. The initial unit cell was indexed using a least-squares analysis of a random set of reflections collected from three series of 0.3° wide ω scans (25 frames/series) that were well distributed in reciprocal space. Data frames were collected [Mo Kα] with 0.3° wide ω scans, 60 s/frame, 606 frames/series. Five complete series were collected with a crystal-to-detector distance of 4.935 cm, thus providing a complete sphere of data to $2\theta_{max} = 50.0°$. A total of 53 909 reflections were collected and corrected for Lorentz and polarization effects and absorption, using Blessing's method as incorporated into the program SADABS, with 14 288 unique [R(int) = 0.0595].

The SHELXTL program package was implemented for data processing, structure solution, and refinement. System symmetry, lack of systematic absences, and intensity statistics indicated the centrosymmetric triclinic space group $P\bar{1}$ (No. 2). The structure was determined by direct methods (XS) with the successful location of the heavy atoms comprising the cluster. After the initial refinement difference Fourier cycle, additional atoms were located and input. After several of these refinement difference Fourier cycles, all of the atoms were refined isotropically and then anisotropically. Disorder was found in the main Sn cluster with two positions found for all of the Sn atoms. The final max/min ratio was 0.82:0.18. Hydrogen atoms were placed in calculated positions. The final structure was refined to convergence ($\Delta/\sigma \leq 0.001$). A final difference Fourier map was featureless, indicating the structure is therefore both correct and complete.

(2) $[K(2,2,2\text{-crypt})]_3[Sn_9Ni_2(CO)]\cdot$en$\cdot(PPh_3)_{0.5}$. A black plate with approximate dimensions 0.521 × 0.312 × 0.026 mm^3 was placed and optically centered on the Bruker SMART CCD system at −80 °C. The data were collected and processed as described above. The SHELXTL program package was again implemented for space group determination and structure solution. System symmetry and systematic absences indicated the unique centrosymmetric monoclinic space group $P2_1/c$ (No. 4). The 314 114 data were merged based upon identical indices yielding 160 194 data [R(int) = 0.0488]. The structure was determined by direct methods with the successful location of nearly all atoms using the program XS. During least-squares refinement the data were truncated to $2\theta_{max} = 50.0°$ with 124 417 data merged to 33 750 unique [R(int) = 0.0477]. After the initial refinement difference Fourier cycle, additional atoms were located and input. A series of difference Fourier refinement cycles eventually completed the assemblage resulting in two disordered $[Sn_9Ni_2(CO)]^{3-}$ clusters, six potassium cryptands, one triphenylphosphine, and two disordered ethylenediamine molecules.

(35) Guo, B. C.; Kerns, K. P.; Castleman, A. W., Jr. *Science* **1992**, *255*, 1411.
(36) Wei, S.; Guo, B. C.; Purnell, J.; Buzza, S.; Castleman, A. W., Jr. *Science* **1992**, *256*, 818.
(37) Fisher, K.; Dance, I.; Willett, G.; Yi, M. N. *J. Chem. Soc., Dalton Trans.* **1996**, 709.

Both of the $[Sn_9Ni_2(CO)]^{3-}$ clusters were disordered but in two different ways. The first is a superposition of two orientations in which the capping Ni atom is in the 1 position (85%) and the 10 position (15%). The centered Ni and several belt Sn atoms are common (or nearly so) to both orientations. The second unique cluster has a similar 0.85:0.15 disorder but the lower population orientation has the Ni(CO) unit in the 6 position. Both of the disordered clusters were successfully modeled giving reasonable and consistent metric parameters. All of the atoms were refined isotropically and then nearly all anisotropically. Hydrogen atoms were placed in calculated positions. The final structure was refined to convergence ($\Delta/\sigma \leq 0.005$). A final difference Fourier map possessed several large unassignable peaks within the heavy atom complexes but was essentially featureless elsewhere, indicating that the structure is therefore complete.

Acknowledgment. This work was supported by the Petroleum Research Fund of the American Chemical Society. We thank Dr. Yiu Fai Lam for assistance with the ^{119}Sn NMR studies, Dr. Brian Balgley for assistance with the ESI-MS studies and Professor Phil DeShong for helpful discussions regarding hydrogenation.

Supporting Information Available: Complete listing of crystallographic data for the three complexes described herein in the form of .cif files. This material is available free of charge via the Internet at http://pubs.acs.org. See any current masthead page for ordering information and Web access instructions.

JA012528P